AD-784 958

RESEARCH IN SEISMOLOGY

W. Stauder, et al

St. Louis University

Prepared for:

Air Force Office of Scientific Research
Advanced Research Projects Agency

1974

Semi-Annual Technical Report
October 1, 1973 - April 30, 1974

ARPA Order No.: 1827-5
Program Code: 3F10
Contractor: Saint Louis University
Effective Date of Contract: 1 March 1973
Contract Expiration Date: April 30, 1975
Amount of Contract: $103,340
Contract Number: F44620-73-C-0042
Principal Investigator: William Stauder
Phone: 314-535-3300-Ext. 540
Program Manager: Same
Short Title: Research in Seismology

Sponsored by

Advanced Research Projects Agency

ARPA Order No. 1827-5

REPORT DOCUMENTATION PAGE

READ INSTRUCTIONS BEFORE COMPLETING FORM

1. REPORT NUMBER: AFOSR - TR - 74 - 1337	2. GOVT ACCESSION NO.
3. RECIPIENT'S CATALOG NUMBER	
4. TITLE (and Subtitle): RESEARCH IN SEISMOLOGY	5. TYPE OF REPORT & PERIOD COVERED: Semi-annual Technical 1 October 73-30 April 74
	6. PERFORMING ORG. REPORT NUMBER
7. AUTHOR(s): W. Stauder, R. Herrmann, R. Street, R. Somayajulu	8. CONTRACT OR GRANT NUMBER(s): F44620-73-C-0042
9. PERFORMING ORGANIZATION NAME AND ADDRESS: Saint Louis University, St. Louis, MO 63108	10. PROGRAM ELEMENT, PROJECT, TASK AREA & WORK UNIT NUMBERS: ARPA Order 1827-5, Program Code 3F10, Program Element 62701E
11. CONTROLLING OFFICE NAME AND ADDRESS: Advanced Research Project Agency/NMR, 1400 Wilson Blvd., Arlington, VA 22209	12. REPORT DATE: 1974
	13. NUMBER OF PAGES: 46
14. MONITORING AGENCY NAME & ADDRESS(if different from Controlling Office): Air Force Office of Scientific Research/NPG, 1400 Wilson Blvd., Arlington, VA 22209	15. SECURITY CLASS. (of this report): Unclassified
	15a. DECLASSIFICATION/DOWNGRADING SCHEDULE

16. DISTRIBUTION STATEMENT (of this Report)

Approved for public release; distribution unlimited.

17. DISTRIBUTION STATEMENT (of the abstract entered in Block 20, if different from Report)

18. SUPPLEMENTARY NOTES

19. KEY WORDS (Continue on reverse side if necessary and identify by block number)

Source parameters
Focal depth
Seismic Scaling Law
Central U.S. earthquakes
Q structure at continental boundary

20. ABSTRACT (Continue on reverse side if necessary and identify by block number)

Matching theoretical and observed Love and Rayleigh spectra allows determination of source parameters including focal depth. Micro to moderate earthquakes in mid-continent scale according to Aki's model A, and evidence a two-fold regional trend, north-south and northwest. The Q structure under the continental boundary of South America indicates complex structure and average low Q.

DD FORM 1 JAN 73 1473 EDITION OF 1 NOV 65 IS OBSOLETE

UNCLASSIFIED

SECURITY CLASSIFICATION OF THIS PAGE (When Data Entered)

Research in Seismology

Semi-Annual Technical Report

Contract F44620-73-C-0042

Table of Contents

Technical Report Summary

This research concerns magnitude determination and the determination of source parameters in a region characteristic of a continental interior. While the ultimate goal is a comparative study of sources of like magnitude in Eurasian source regions, the proximate purpose has been a better understanding, first, of seismic source parameters in the mid-continent United States. This report completes this phase of the investigation, and presents results in three areas of inquiry.

1. A technique has been developed whereby theoretical Love and Rayleigh amplitude spectra can be generated for an assumed earth model for a given choice of five source parameters: the strike, dip, and slip angles, focal depth and seismic moment. The parameters are systematically varied to find the best agreement between observed and theoretical spectra for the entire range of the observed spectra. The method has been applied to determine the source parameters for 10 central U. S. earthquakes with $M_o \cong 10^{22}$ dyne-cm.

2. Other studies of earthquakes of the central U. S. have resulted in a seismic scaling law for earthquakes in the moment range 10^{18} through 10^{24} dyne-cm which resembles Aki's revised model A theoretical law but displaced toward shorter periods. Dependence is shown on the period at which

m_b is determined in the m_b vs M_o relation. Focal mechanisms of 38 of these events show a complicated regional stress pattern with two principal trends: a north-south trend along which high angle normal faulting changes to high angle reverse faulting, and a northwest trend of normal faults.

3. The spectral ratio of pP/P from deep focus earthquakes in South America yields generally low values of $\overline{Q}$ ($Q \cong 400$) for the region above the focus, with systematic differences for segments of path along rays to western U.S., for which $\overline{Q}$ is lower and more erratic, and the eastern U.S., for which $\overline{Q}$ is more stable. The low value of $\overline{Q}$ is an average value and may result from both low and high Q structures under South America.

A Technique for Determining Earthquake Source Parameters by Using Surface Wave Amplitude Spectra.

by Robert B Herrmann

An effective method for the determination of the strike, dip, and slip angles, focal depth, and seismic moment by using the fundamental mode amplitude spectra of Love and Rayleigh waves has been developed. The approach taken is to find the particular combination of these source parameters which gives the best agreement between the observed and theoretically predicted surface wave amplitude spectra at all observing stations for the entire period range of the observed spectra.

Using the development of surface wave theory by Tsai and Aki (1970), theoretical Love and Rayleigh amplitude spectra can be generated from an assumed earth model for a given choice of the five source parameters. We assume that the dislocation source is a step function in time.

Let $y_L(T,\phi)$ and $y_R(T,\phi)$ be the observed Love and Rayleigh wave amplitude spectra of a particular mode at a period T and azimuth ϕ which have been corrected for the geometrical spreading of surface waves on a sphere to a reference distance of 9° (1000 km) and also corrected for the decrease in amplitude due to the effects of anelastic attenuation. If A_Q is the observed amplitude spectrum of the Q wave type at a distance Δ from the source and Y_Q

is the appropriate anelastic attenuation coefficient, then the corrected amplitude spectrum is

$$y_Q = A_Q \left(\frac{\sin \Delta}{\sin 9^o} \right)^{\frac{1}{2}} \exp(\gamma_Q \Delta) .$$

For a given choice of the source parameters, strike (STRK), dip (DIP), slip (SLIP), and depth (H), theoretical amplitude spectra can be generated at a reference distance of 9^o for a unit dislocation source such that for each observed $y_Q(T,\emptyset)$, a corresponding theoretical amplitude spectrum $x_Q(T,\emptyset)$ can be predicted. Thus for each data point of the observed amplitude spectrum specified by its period, azimuth, and mode, there corresponds a predicted amplitude for the same period, azimuth, and mode. Having established this one-to-one relationship, we will drop the $(T,\emptyset)$ description of the observed and predicted spectra and just consider the y_{Qj} and x_{Qj} observational-theoretical pair, where the j index indicates a particular y_Q - x_Q pair from the data set of all observed periods and azimuths.

Let there be a total of NL Love wave observations of the amplitude spectrum and NR Rayleigh wave observations. The data sets consist of the totality of Love and Rayleigh wave spectral amplitude observations available in the range of observed periods at all azimuths. Using the simplified notation, the following parameters are defined:

$$RL = \frac{\sum_{j=1}^{NL} (x_{Lj} - \bar{x}_L)(y_{Lj} - \bar{y}_L)}{\left\{ \sum_{j=1}^{NL} (x_{Lj} - \bar{x}_L)^2 \sum_{j=1}^{NL} (y_{Lj} - \bar{y}_L)^2 \right\}^{1/2}}$$

where

$$\bar{x}_L = \frac{1}{NL} \sum_{j=1}^{NL} x_{Lj} \ , \ \bar{y}_L = \frac{1}{NL} \sum_{j=1}^{NL} y_{Lj} \ ;$$

$$RR = \frac{\sum_{j=1}^{NR} (x_{Rj} - \bar{x}_R)(y_{Rj} - \bar{y}_R)}{\left\{ \sum_{j=1}^{NR} (x_{Rj} - \bar{x}_R)^2 \sum_{j=1}^{NR} (y_{Rj} - \bar{y}_R)^2 \right\}^{1/2}}$$

where

$$\bar{x}_R = \frac{1}{NR} \sum_{j=1}^{NR} x_{Rj} \ , \quad \bar{y}_R = \frac{1}{NR} \sum_{j=1}^{NR} y_{Rj} \ ;$$

$$ML = \frac{\sum_{j=1}^{NL} x_{Lj} \, y_{Lj}}{\sum_{j=1}^{NL} x_{Lj}^2}$$

$$MR = \frac{\sum_{j=1}^{NR} x_{Rj}\, y_{Rj}}{\sum_{j=1}^{NR} x_{Rj}^2}$$

$$MO = \frac{NR \cdot MR + NL \cdot ML}{NR + NL}$$

$$RESL = \sqrt{\sum_{j=1}^{NL} \frac{(y_{Lj} - MO \cdot x_{Lj})^2}{NL}}$$

$$RESR = \sqrt{\sum_{j=1}^{NR} \frac{(y_{Rj} - MO \cdot x_{Rj})^2}{NR}}$$

$$RES = \left[\frac{NL \cdot RESL \cdot RESL + NR \cdot RESR \cdot RESR}{NL + NR} \right]^{1/2}$$

The significance of these parameters is as follows. The RL and RR are correlation coefficients between the observed and theoretical Love and Rayleigh wave data sets. The correlation coefficient is not affected by multiplicative scaling, e.g. seismic moment, but rather gives a measure of the similarity of the observed and theoretical azimuthal radiation patterns over the entire period range of the observations. ML and MR are, respectively, least squares estimates of the seismic moment using the Love and Rayleigh wave data sets independently. MO is the weighted estimate of the seismic moment.

RESL and RESR are the root mean square amplitude spectrum residuals between the observed amplitude spectra and the theoretical predictions made using the average seismic moment MO. RES is the root mean square amplitude spectrum residual for the entire data set.

The technique for selecting the source parameters which best describe the surface wave observations follows. For each particular choice of SLIP, DIP, STRK, and H, the following quantities are computed and displayed: MO, RR, RESR, MR, RL, RESL, ML and RES. The best focal mechanism and focal depth combination is taken to be the one for which the correlation coefficients RR and RL are as large as possible and for which the seismic moment estimates ML and MR are also as close as possible. Usually it happens that for the source parameters satisfying these criteria, RESL, RESR, and RES are also minimal. The advantage of this algorithm is that equal weight is given to the Rayleigh and Love wave observations and that noise in one data set does not unduly affect the best choice made by the other data set. A disadvantage is that the systematic search is very time consuming on a digital computer, as opposed to iterative methods.

The search is usually begun over the following parameter space:

SLIP	-90°	(20°)	70°
DIP	30°	(15°)	90°
STRK	0°	(20°)	160°
H	0	(5)	25 km .

The numbers within the parentheses indicate the incrementing value used in going from the smallest to the largest value of the particular parameter. Due to the symmetry of the surface wave radiation pattern to a 180° rotation for a double-couple seismic source and because only amplitudes are being used, these search limits encompass all possible focal mechanisms.

Once a solution region is located, a finer search grid is used until all angles are known to within 5° and the depth is known to within 2 kilometers. Usually the results of this technique are not a single best solution, but rather a suite of possible solutions to the surface wave amplitude problem. The choice of the focal mechanism of the earthquake is taken to be that member of the suite of possible solutions which gives the best fit to the P wave first motion data.

References

Tsai, Y. B. and K. Aki (1970). Precise focal depth determination from amplitude spectra of surface waves, J. Geophys. Res. 75, 5729-5743.

Appendix. A Summary of Central United States Earthquake Source Parameters Determined from Surface Wave and P Wave Observations.

by Robert B. Herrmann

In the previous section, a systematic search procedure for the determination of earthquake source parameters using surface wave amplitude spectra was discussed. The results of applying this method to the data available from some central United States earthquakes are presented.

The amount of data available for the surface wave studies depended on the size of the earthquake studied and the number of seismograms available for the event. The 14 August 1965 event was recorded at eleven long period seismograph stations. There were 88 Rayleigh wave and 91 Love wave spectral amplitude observations available in the 2-12 second period range. On the other hand the 03 March 1963 event had 529 Rayleigh wave observations in the 7-50 second period range from 36 stations and 393 Love wave observations in the 8-50 second period range from 28 stations. For the other events studied there were on the average 250 Love and Rayleigh wave spectral amplitude observations in the 8-50 second period range from 20 stations.

In analyzing the data, an attenuation model which represented an average of the models of Mitchell (1973) and Herrmann (1973) was used to correct for the effects of anelastic attenuation on the observed amplitudes. The

seismic source was assumed to be of the step dislocation in time type.

The results of our investigation are presented in Table I. This table lists the date and origin time of the event together with the epicentral coordinates. The orientations of the nodal planes and the orientations of the pressure and tension axes as determined by the joint use of surface wave and P wave data are also listed. The surface wave observations made possible an estimate of the focal depth and the seismic moment. The m_b and M_S magnitudes for each event are from Nuttli and Zollweg (1974). As a result of the investigations made, the seismic moment is estimated to be accurate to within a multiplicative factor of 1.5, the focal depth to within 2.5 kilometers, and the nodal plane strike and dip to within 10^o.

Further studies will be made relating the seismic moment and magnitude with a careful appraisal of any discrepancies which might occur.

References

Herrmann, R. B. (1973). Surface-wave generation by the south central Illinois earthquake of November 9, 1968, Bull. Seism. Soc. Am. 63, 2121-2134.

Mitchell, B. J. (1973). Surface-wave attenuation in central North America, Bull. Seism. Soc. Am. 63, 1057-1071.

Nuttli, O. W. and J. E. Zollweg (1974). The relation between felt area and magnitude for central United States earthquakes, Bull. Seism. Soc. Am. 64, 73-85.

Table 1

Summary of Source Parameters

Date	OT(UT)	Lat (°)	Lon (°)	Plane a Stk Dip	Plane b Stk Dip	P Axis Trn Pl	T Axis Trn Pl	m_b	M_S	M_o dyne-cm	H km
02 Feb 62	06 43 34.0	36.5N	89.6W	340 75E	99 29S	52 26	278 54	4.3	3.5	2.6E22	8
03 Mar 63	17 30 11.4	36.7	90.1	220 60W	122 77S	174 10	76 31	4.8	4.1	7.7E22	13
14 Aug 65	13 13 56.6	37.2	89.3	197 71E	280 70N	237 17	147 1	3.8	2.5	1.4E21	1
21 Oct 65	02 04 38.3	37.5	91.0	260 40N	55 53S	278 79	161 6	4.9	4.1	6.9E22	5
04 Jun 67	16 14 13.6	33.6	90.9	20 80W	294 70N	248 7	156 22	4.5	3.0	3.0E22	10
21 Jul 67	09 14 48.9	37.5	90.4	350 60E	107 52S	314 52	50 5	4.3	2.8	1.2E22	15
09 Nov 68	17 01 42.0	38.0	88.5	359 47E	15 45W	97 1	192 82	5.5	5.2	9.0E23	20
01 Jan 69	23 35 36.2	34.8	92.6	260 55N	35 45E	330 7	228 65	4.4	3.3	3.8E22	9
17 Nov 70	02 13 55.1	35.9	89.9	220 75W	319 17E	270 10	173 32	4.4	2.9	1.1E22	14
15 Sep 72	05 22 15.5	41.6	89.4	350 70W	267 71N	38 0	128 28	4.4	3.3	1.7E22	13

2. The Seismic Scaling Law and Source Mechanism Characteristics for Small Magnitude Events in the Central United States.

by Ronald Street

The objective of this report is to outline the results of recent research directed towards characterizing earthquake activity in the six-state area of Illinois, Missouri, Tennessee, Arkansas, and Kentucky. With this objective in mind, source characteristics of some eighty earthquakes, and the focal mechanisms of more than thirty of the larger of these, have been determined.

The principal result of that portion of the study concerned with source characteristics has been the establishment of a scaling law of the source-time function involving displacement spectral densities from the excitation of the Lg waves (as observed on short-period records) for earthquakes whose seismic moment ranges from 10^{18} through 10^{24} dyne-cm. The principal result of the portion involving focal mechanisms has been the establishment of two generalized trends of earthquake mechanisms which appear to be closely related to local tectonic features such as the Mississippi Embayment, the Ozark Uplift, and the Pascola Arch. Data for both studies were gathered from seismograms of the Long Range Seismic Measurement (LRSM) stations, the World Wide Standardized Seismic Network (WWSSN), Saint Louis University stations, and individual stations operated by nearby universities (see Fig. 1).

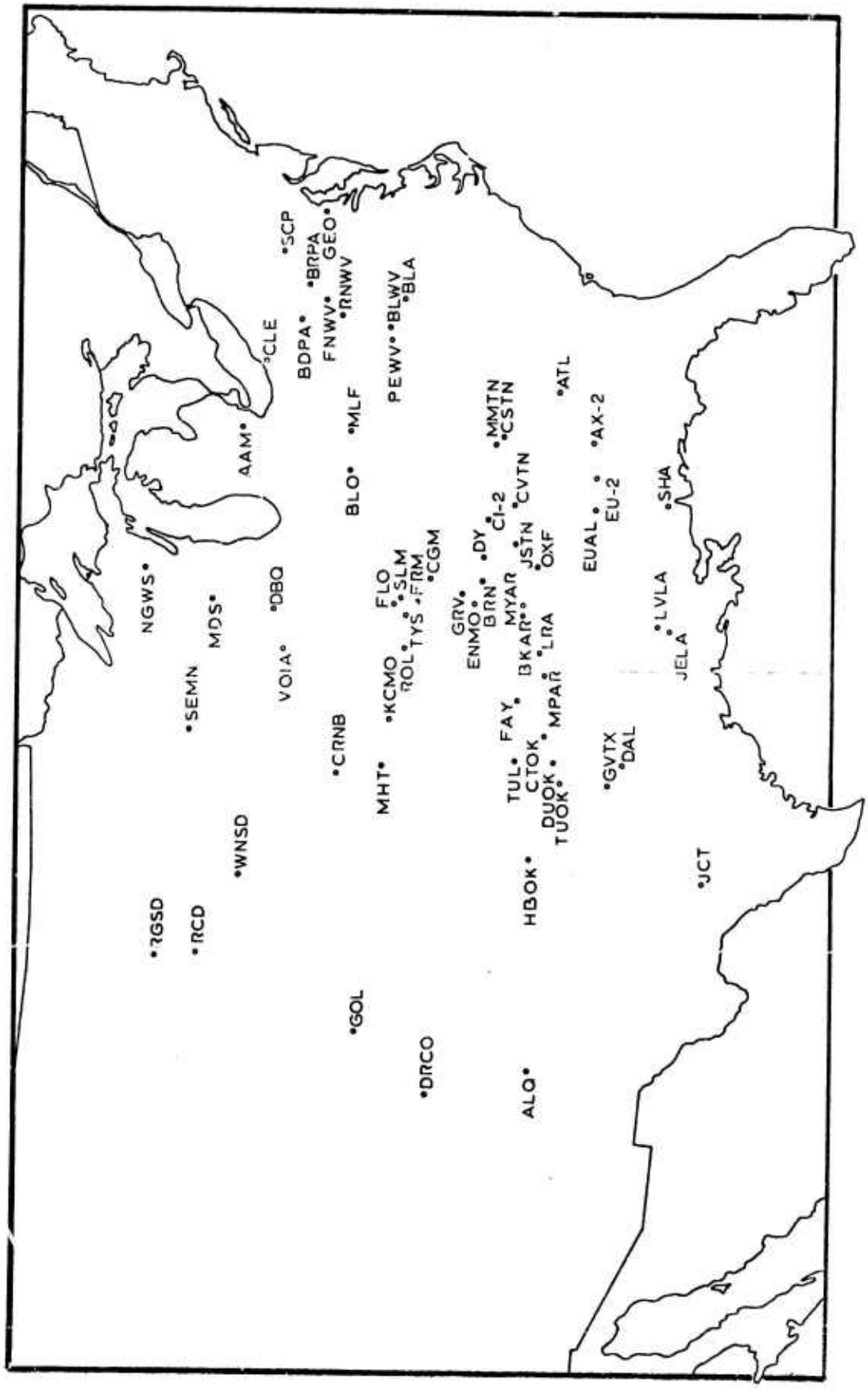
SCP
BRPA
GEO
RNWV
BLWV
BLA
BDPA
FNWV
CLE
PEWV
MLF
ATL
MMTN
CSTN
AAM
AX-2
BLO
CVTN
CI-2
EU-2
SHA
EUAL
DY
JSTN
OXF
CGM
SLM
FLO
NGWS
DBQ
GRV
ENMO
BRN
MYAR
BKAR
LRA
LVLA
JELA
MDS
SEMN
VOIA
KCMO
ROL
TYS
FAY
MPAR
GVTX
DAL
CRNB
MHT
TUL
CTOK
DUOK
TUOK
HBOK
JCT
7GSD
RCD
WNSD
GOL
DRCO
ALO

Figure 1

Concerning the source-time function, the procedure followed was first to determine the displacement spectral density of an earthquake's coda beginning with the maximum trace offset after the P phase arrivals. For the spectral analysis codas were digitized from this point on the trace until such time that they were substantially less than the initial maximum sustained motion. At small epicentral distances the maximum trace offset in the earthquake's coda, excluding the P phases, was the Sg phase, while for distances of approximately 100 km or more the maximum trace offset, and the point at which digitizing was begun, was the Lg phase. However, since all but the very smallest of events (those with moment $< 10^{19}$ dyne-cm) were principally based on data taken at epicentral distances greater than 100 km, the derived displacement spectral density will commonly be referred to as that of the Lg phase.

Once the Lg displacement spectral densities were determined, the observed zero frequency levels for eight large events for which Herrmann (1974) had determined the seismic moment were noted. Then using as the definition of seismic moment

$$M_o = 4\pi\rho\beta^3 R\Omega_o \qquad \text{where} \begin{cases} \rho = \text{density} \\ \beta = \text{shear wave velocity} \\ \Omega_o = \text{zero frequency level} \\ R = \text{reference distance} , \end{cases}$$

a new parameter designated as the spectral density level (hereafter denoted by S.D.L.) was empirically equated to the seismic moment by a suitable modification of R. Values

used for ρ and β were 2.5 gm/cm^3 and 3.5 x 10^5 cm sec respectively. Once the S.D.L. had been corrected to agree with the seismic moment for the eight larger events, the nature of R as a function of the epicentral distance was investigated by comparing the S.D.L. from stations varying in distances of 20 to 400 km. The resulting equations of the S.D.L. for events studied in this report were determined to be

$$\text{S.D.L.} = \begin{cases} 1.34\ (\times 10^{25})\ r/100 & r \leq 100 \text{ km} \\ 1.34\ (\times 10^{25})\ \sqrt{r/100} & r \geq 100 \text{ km} \end{cases} \quad (=M_o)$$

where r is the epicentral distance in km and the values of ρ and β are as previously indicated. Physically this means that the displacement spectral density determined for an event is corrected as a body wave for epicentral distances less than 100 km, whereas for greater distances, it is treated in the manner of a surface wave correction. In this manner, the gross spectral properties of more than eighty earthquakes were determined so as to be consistent with those events whose seismic moments were found by Herrmann. Fig. 2 illustrates a number of these events, indicating zero frequency levels, corner periods, and a variety of falloff behaviors.

Fig. 3 is a plot of the observed w^{-2} spectral corner period vs the displacement spectral density levels for many of the events shown in Fig. 2. In the case of an event exhibiting two spectral corners the w^{-2} falloff was extrapolated to the zero frequency level. The slope of the upper

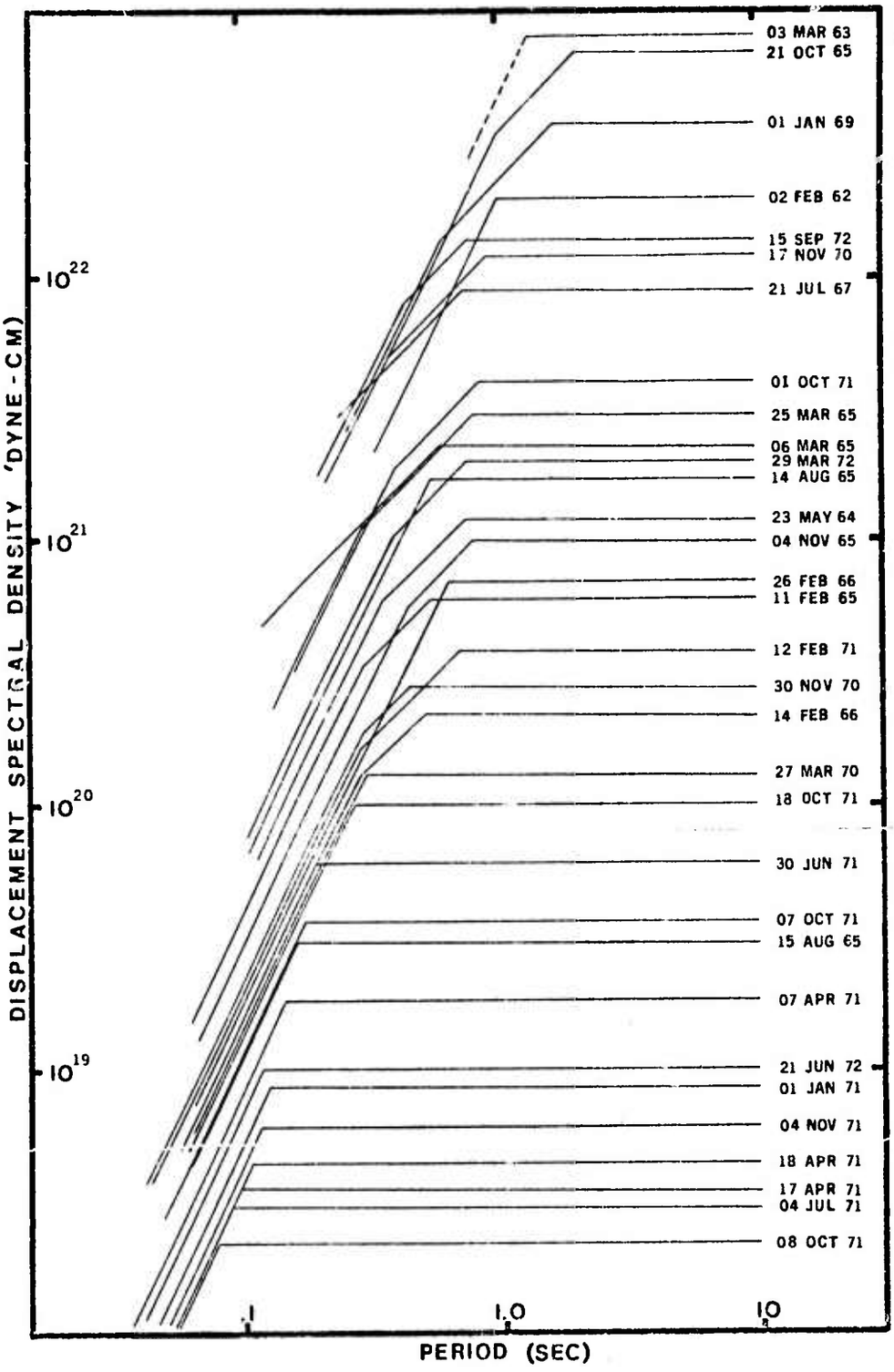
03 MAR 63
21 OCT 65
01 JAN 69
02 FEB 62
15 SEP 72
17 NOV 70
21 JUL 67
01 OCT 71
25 MAR 65
06 MAR 65
29 MAR 72
14 AUG 65
23 MAY 64
04 NOV 65
26 FEB 66
11 FEB 65
12 FEB 71
30 NOV 70
14 FEB 66
27 MAR 70
18 OCT 71
30 JUN 71
07 OCT 71
15 AUG 65
07 APR 71
21 JUN 72
01 JAN 71
04 NOV 71
18 APR 71
17 APR 71
04 JUL 71
08 OCT 71
10^{22}
10^{21}
10^{20}
10^{19}
DISPLACEMENT SPECTRAL DENSITY 'DYNE-CM)
.1
1.0
10
PERIOD (SEC)

Figure 2

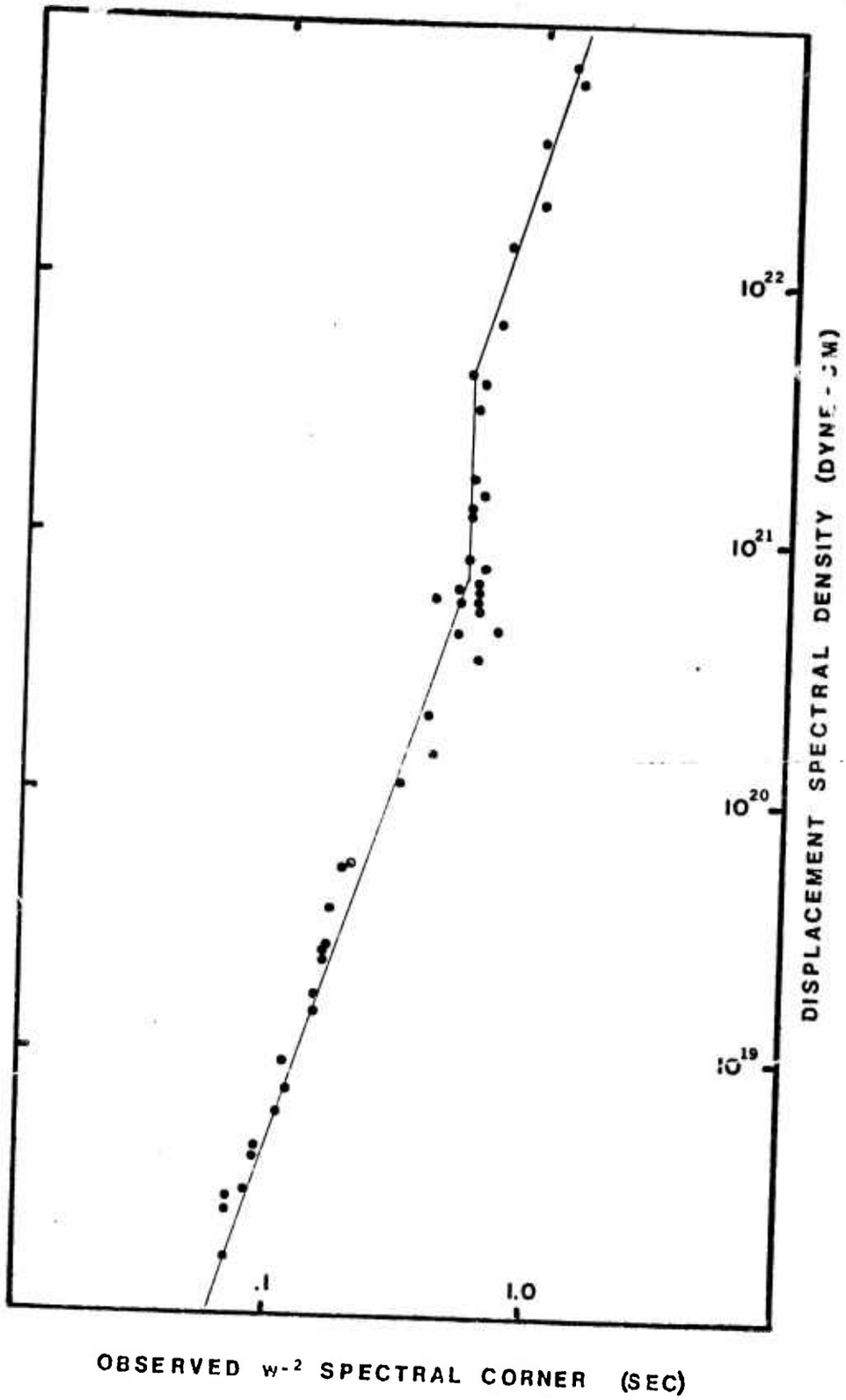
10^{22}
10^{21}
10^{20}
10^{19}
DISPLACEMENT SPECTRAL DENSITY (DYNE-CM)
.1
1.0
OBSERVED w^{-2} SPECTRAL CORNER (SEC)

Figure 3

and lower line segments in Fig. 3 is w^{-3}. It is interesting to note that the three line segments indicated are remarkably similar to Aki's (1972) revised model A theoretical scaling law (see Aki's Fig. 9). However, it should also be noted that the plot obtained from observational data for this report differs from Aki's in an important respect; the observational plot in Figure 3 is displaced towards shorter periods and at a greater S.D.L. when compared to Aki's model A. This fact is significant if we are to relate the three quantities M_S, m_b, and M_o; two of these quantities, M_o and m_b, are plotted as functions of each other in Fig. 4. Also shown in Fig. 4 is the variation of m_b with the magnitude of the same event for the 0.33 and 0.1 period waves in addition to the 1.0 period waves.

The next step was to determine the correctness of the magnitude relationships as proposed by Nuttli (1973) by plotting a number of the better determined events as a function of their displacement spectral density levels. Fig. 5 shows the result. The broken and solid lines are two different least squares fits to the data shown. The broken line is the least squares fit to all the data, while the solid line is the least squares fit to the data considered as being made up of two groups with moments greater and less than 10^{21} dyne-cm, respectively. Using either of the two cases, it appears that for events whose S.D.L. is less than approximately 10^{22} dyne-cm, the magnitude is progressively overestimated as the size of the events decreases.

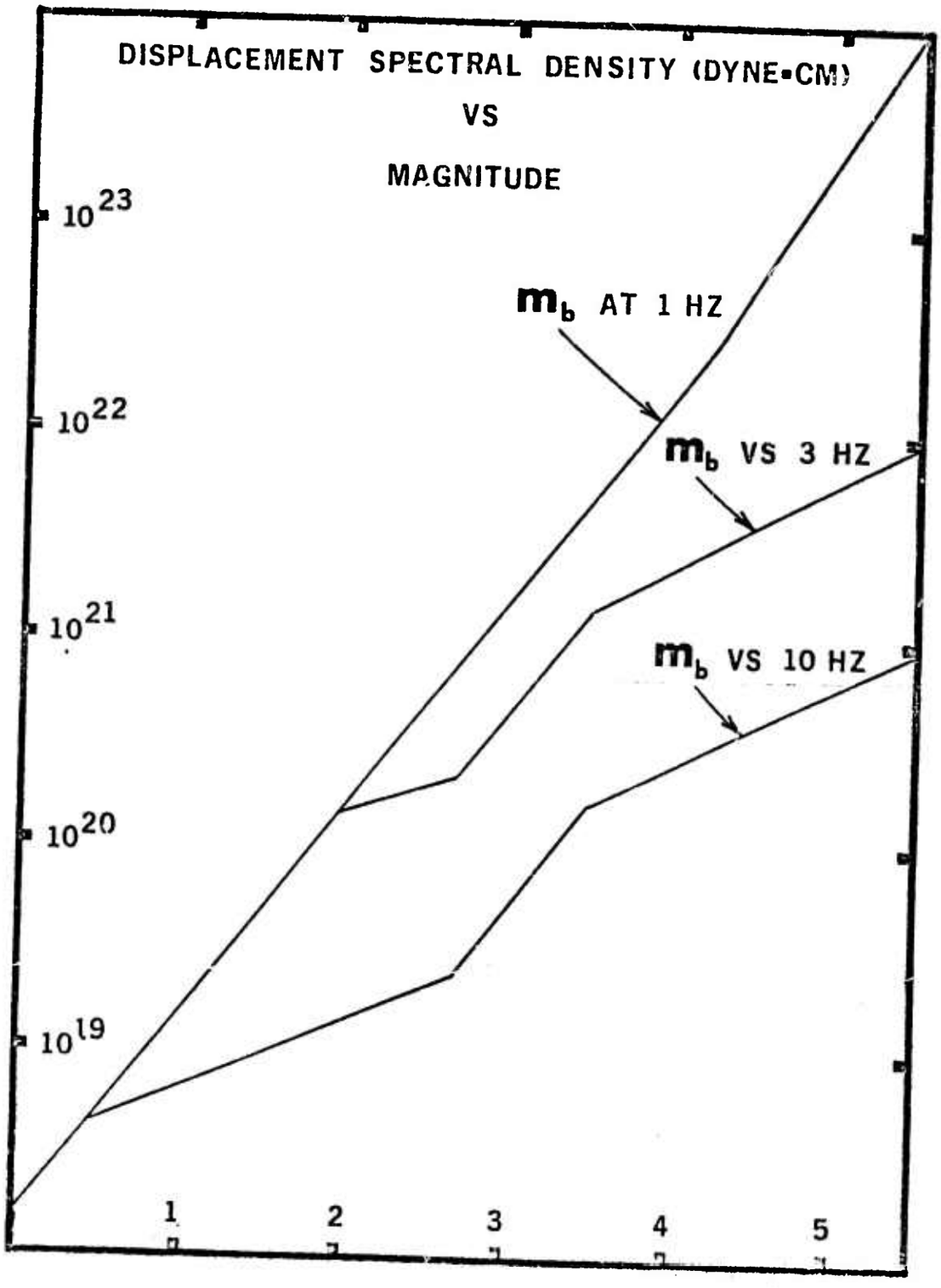
DISPLACEMENT SPECTRAL DENSITY (DYNE•CM)
VS
MAGNITUDE
10^{23}
10^{22}
10^{21}
10^{20}
10^{19}
m_b AT 1 HZ
m_b VS 3 HZ
m_b VS 10 HZ
1
2
3
4
5

Figure 4

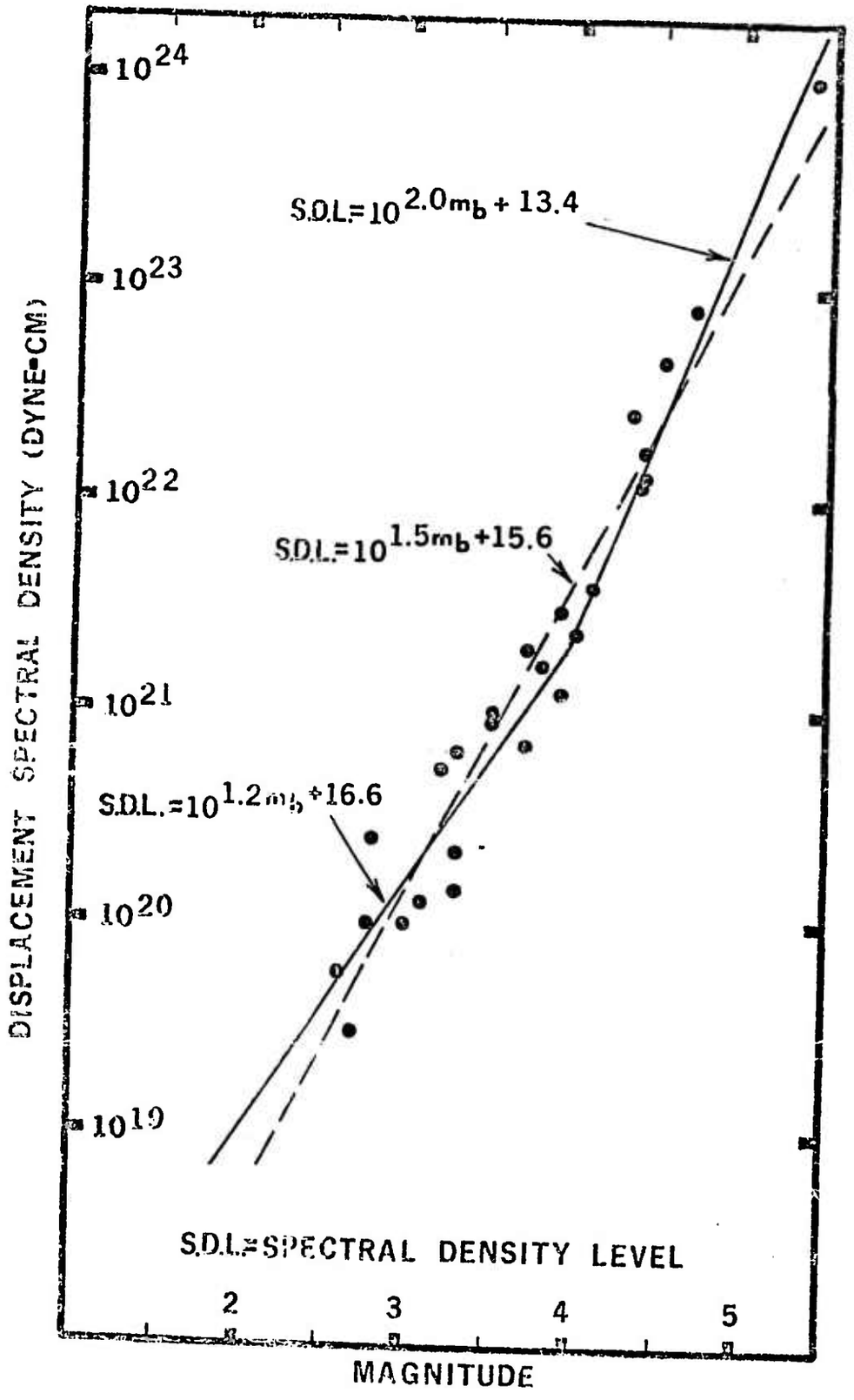
10^{24}
10^{23}
10^{22}
10^{21}
10^{20}
10^{19}
S.D.L=$10^{2.0m_b + 13.4}$
S.D.L=$10^{1.5m_b+15.6}$
S.D.L.=$10^{1.2m_b+16.6}$
DISPLACEMENT SPECTRAL DENSITY (DYNE•CM)
S.D.L=SPECTRAL DENSITY LEVEL
2
3
4
5
MAGNITUDE

Figure 5

This is the result of the break in the slope of the m_b vs S.D.L. scaling near the 10^{22} dyne-cm S.D.L., and the failure of Nuttli's magnitude relationship to reflect the change in the displacement spectral density spectrum observed at the 1.0 second period for earthquakes with S.D.L. less than 10^{22} dyne-cm. This overestimation of magnitude could significantly modify the m_b vs felt area (Nuttli and Zollweg, 1973), and the recurrence relationships (Nuttli, 1973) for central United States.

The second part of this research effort involved a detailed focal mechanism investigation of moderate size earthquakes occurring during the last thirteen years and within the six-state region of interest. The events studied are listed chronologically in Table 1. Figure 6 illustrates the focal mechanisms determined for these events from the first motion of P. The mechanism solutions shown include those of Herrmann (1974), which were obtained from the consideration of the amplitude spectrum of surface-wave motion, as well as the thirty solutions based on the sense of motion of crustal P phases (Pn, P*, Pg) determined for this report. For those events based on the sense of motion, compressions or dilations were plotted on the lower hemisphere of an equal area stereographic projection at the appropriate azimuth and incidence angle. Depending on the particular event, it is felt that the errors in the strike and dip of the nodal planes are no more than 10 - 20°.

Table 1. Focal mechanism parameters for Central United States earthquakes.

EVENT	DATE	OT(UT)	LAT (° N)	LON (° W)	P AXIS		T AXIS	
					TREND	PLUNGE	TREND	PLUNG
1	02 FEB 62	06 43 34.0	36.5	89.6	52	26	278	54
2	01 JUN 62	11 23 40.5	35.0	90.2	336	80	252	0
3	14 JUL 62	02 23 49.0	36.8	89.9	92	2	356	82
4	23 JUL 62	06 05 17.0	36.1	89.4	131	75	233	5
5	03 MAR 63	17 30 11.4	36.7	90.1	174	10	76	31
6	31 MAR 63	13 31 03.7	36.9	89.0	161	83	104	0
7	06 APR 63	08 12 22.4	36.5	89.6	85	7	346	56
8	03 AUG 63	02 37 47.8	37.0	88.7	92	3	191	83
9	16 JAN 64	05 09 57.1	36.8	89.5	220	15	95	60
10	17 MAR 64	02 15 29.0	36.2	89.6	304	32	168	48
11	23 MAY 64	15 00 33.7	36.6	90.0	223	68	83	12
12	11 FEB 65	03 40 24.0	36.4	89.7	268	10	33	67
13	06 MAR 65	21 08 50.5	37.5	91.1	260	67	165	0
14	14 AUG 65	13 13 56.6	37.2	89.3	238	27	147	1
15	21 OCT 65	02 04 38.4	37.5	91.1	340	85	160	5
16	04 NOV 65	07 43 33.6	37.1	91.0	156	5	289	83
17	12 FEB 66	04 32 14.7	35.9	90.0	140	83	271	5
18	13 FEB 66	23 19 36.9	37.0	91.0	292	68	183	7
19	26 FEB 66	08 10 19.4	37.1	91.0	292	68	183	7
20	06 DEC 66	08 00 47.0	38.9	92.8	277	2	10	58
21	04 JUN 67	16 14 13.6	33.6	90.9	248	7	156	22
22	21 JUL 67	09 14 48.9	37.5	90.6	314	52	50	5

Table 1. Cont'd.

EVENT	DATE	OT(UT)	LAT (° N)	LON (° W)	P AXIS TREND	P AXIS PLUNGE	T AXIS TREND	T AXIS PLUNGE
23	09 NOV 68	17 01 42.0	38.0	88.5	97	1	192	82
24	01 JAN 69	23 35 36.2	34.8	92.6	330	7	228	65
25	28 FEB 69	13 10 13.1	37.9	88.6	282	2	192	78
26	27 MAR 70	03 44 29.5	36.5	89.7	264	75	15	8
27	17 NOV 70	02 13 54.5	35.9	90.2	71	67	307	13
28	12 FEB 71	12 44 27.2	38.5	87.9	78	50	344	3
29	13 APR 71	14 00 50.0	35.8	90.1	54	72	263	15
30	18 OCT 71	06 39 30.7	36.7	89.6	108	8	12	53
31	01 FEB 72	05 42 10.0	36.4	90.8	227	60	128	10
32	29 MAR 72	20 38 31.9	36.2	89.6	180	86	270	10
33	07 MAY 72	02 12 08.5	35.9	90.0	52	72	265	15
34	09 JUN 72	19 15 19.1	37.7	90.4	269	49	15	14
35	19 JUN 72	05 46 14.7	37.0	89.1	138	22	268	60
36	12 JAN 73	11 56 56.0	37.9	90.5	70	25	278	63
37	03 OCT 73	03 50 14.0	35.8	90.1	251	13	114	72
38	09 OCT 73	20 18 26.8	36.5	89.6	36	15	263	67

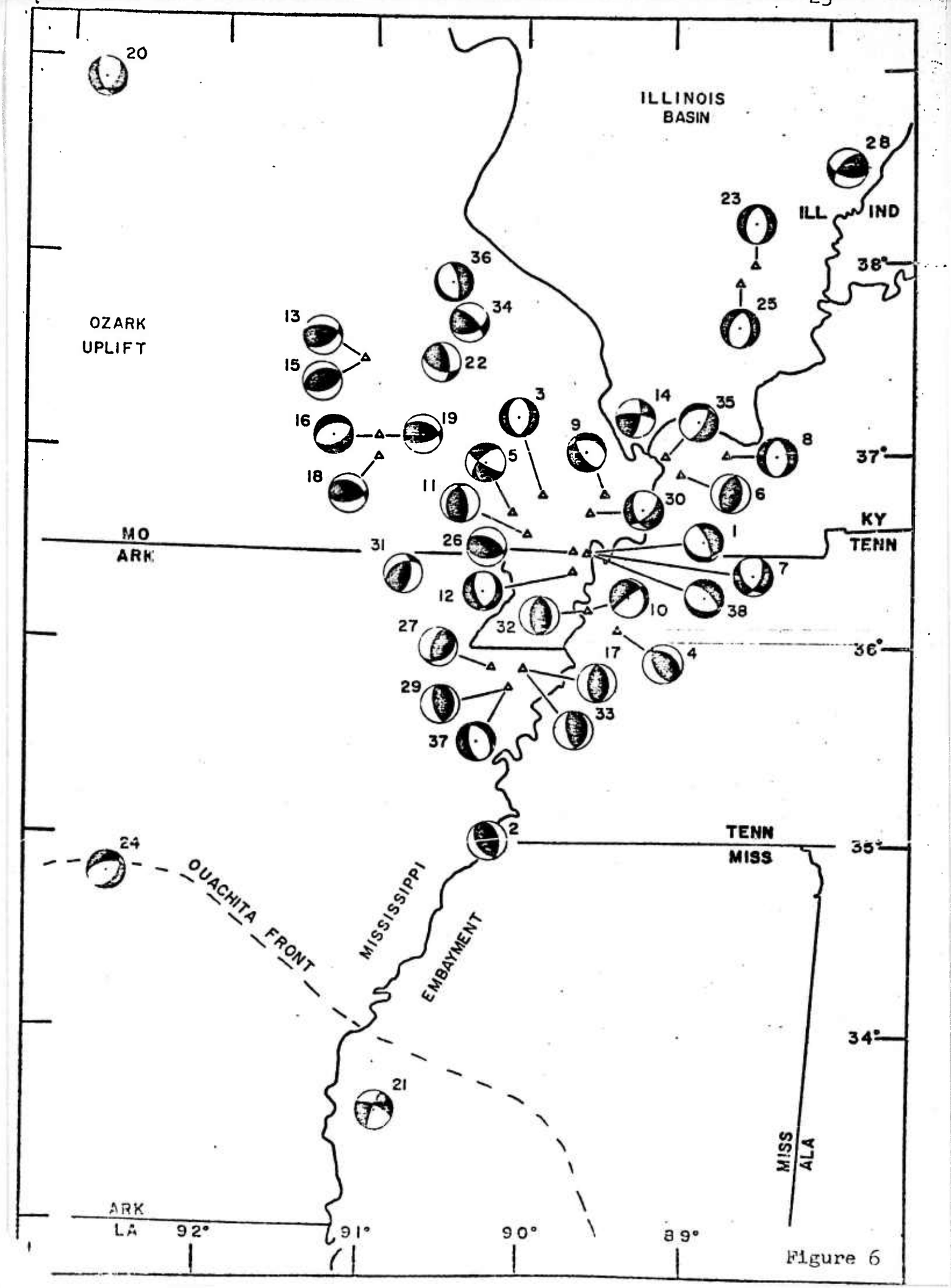
ILLINOIS
BASIN
OZARK
UPLIFT
MO
ARK
KY
TENN
ILL
IND
TENN
MISS
MISS
ALA
ARK
LA
OUACHITA FRONT
MISSISSIPPI
EMBAYMENT
38°
37°
36°
35°
34°
92°
91°
90°
89°

Figure 6

Focal mechanisms done by Herrmann (1, 5, 14, 15, 21, 22, 23, and 24) were obtained by the assumption of a hypothetical event which was then varied until the theoretical radiation patterns for Love and Rayleigh waves compared favorably to those actually observed. A constraint on the chosen solution is that it must be in reasonable agreement with the observed sense of motion of the various P phases. Errors in the strike and dip of the nodal planes, as determined by this method, are probably less than 10^{o}. While this is obviously a superior method to that which uses P wave data only, it is restricted to events which excite fundamental mode surface waves in the 4 to 50 second period range sufficiently so that they are measurable on long-period seismograms.

The strike of the nodal planes shown in Fig. 6, with a few exceptions, can be grouped into two trends. The most prominent is a group of earthquakes whose nodal planes strike nearly north-south and whose epicenters extend northward from Memphis, Tennessee through central Illinois. The second grouping of earthquakes whose nodal planes appear to correlate with one another are those in central Missouri. The strike of the nodal planes of this group tend northwest-southeast.

Two significant points to be noted about these two trends are the complexity of their intersection, and the change in character of the north-south trend from high-angle normal faulting south of 36.3^{o}N (near the buried

Pascola Arch) to high-angle thrust faulting to the north. The focal mechanisms in the vicinity of the intersection of the two trends, as indicated by the mechanism diagram on the figure, is complex.

The complexity of the focal mechanisms near the intersection of the two trends was supported by an attempt to resolve a composite fault plane solution involving twenty-two microearthquakes occurring in the immediate vicinity of $36.5^{\circ}N/89.4^{\circ}W$. Based on the sense of first motions at five seismographs (GRV, BRM, DY3, DY4, and DY5) located in the area surrounding this point, it proved to be impossible to separate the composite fault plane stereographic projection into any reasonable number of solutions. This supports the contention of intersecting fault zones as well as implying something other than a simple stress field as the cause of observed earthquake activity in this region.

As for the change in the character of faulting in the north-south trend, the implication is that this continuous trend of earthquake epicenters is characterized by a tensional stress system predominating in the southern portion and a compressive stress system predominating in the north.

Three mechanisms, those of 03 Mar 63, 01 Jan 69, and 14 Aug 65, have a possibly interesting interpretation. All three occur near the intersections of nodal-plane trends. Fig. 7 illustrates the two trends previously described and the three strike-slip focal mechanisms listed above. While the relationship of the events of

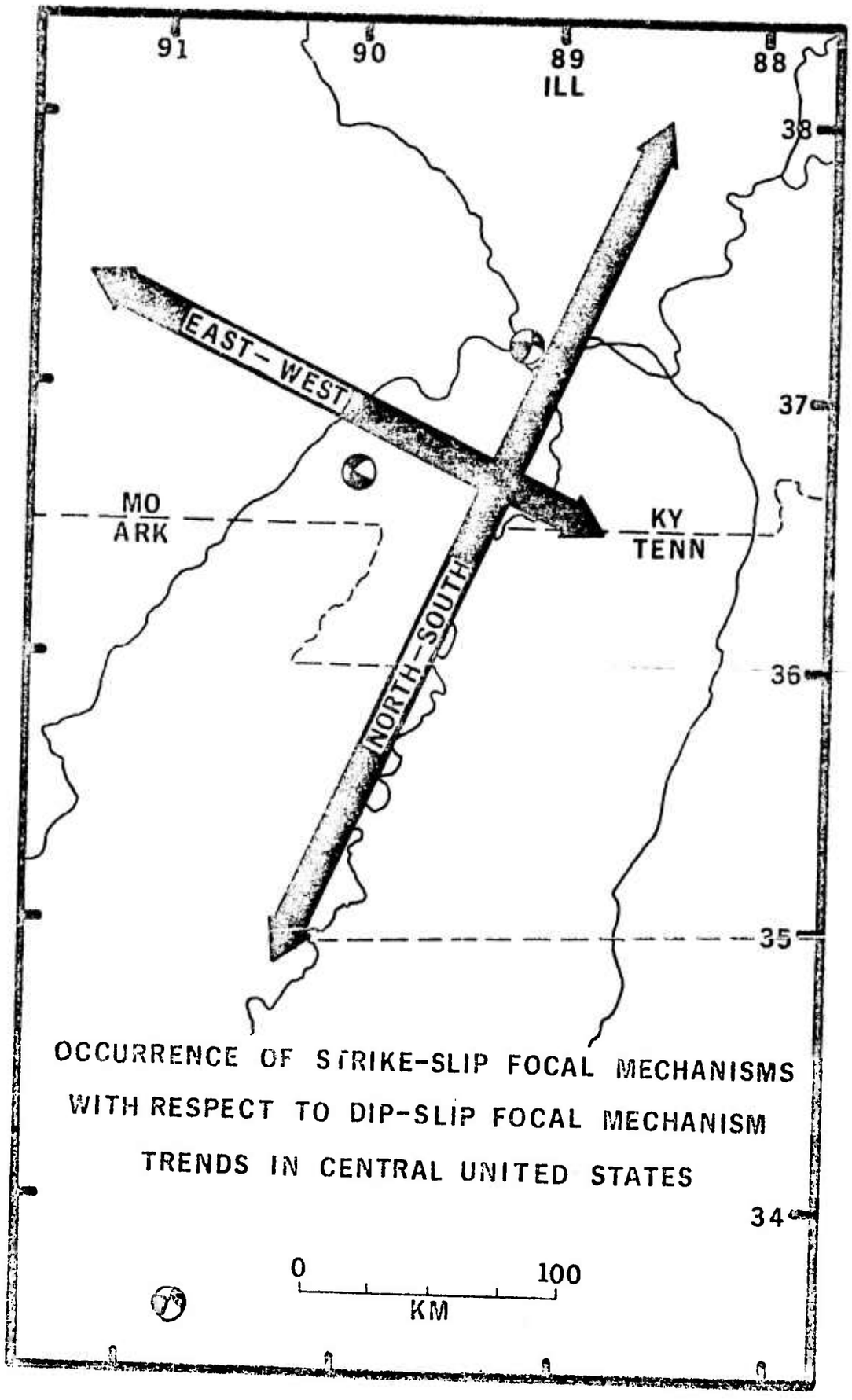

OCCURRENCE OF STRIKE-SLIP FOCAL MECHANISMS WITH RESPECT TO DIP-SLIP FOCAL MECHANISM TRENDS IN CENTRAL UNITED STATES

Figure 7

03 Mar 63 (No. 5) and 14 Aug 65 (No. 14) to the intersection of the two trends is clear, that of the 01 Jan 69 event (No. 24) is not. However, if Oetking's (1966) description of the Ouachita Front as being a thrust feature is accepted, then the mechanism of this event could be the result of a superposition of the thrust fault, compressive-stress system associated with the Ouachita Front and the perpendicular normal fault, tensional-stress as found at Memphis. This hints at the possibility of tensional-type faulting extending southward from Memphis along the axis of the Mississippi Embayment to the Ouachita Front. But at present the distribution of seismograph stations is not adequate to determine if earthquakes are occurring along such an extension.

The results of the research presented in this report bear on three important problems: the source time function of micro- and moderate-size earthquakes, the state of stress in the interior of a continental lithospheric plate, and the relation of present-day earthquake activity in the central United States to geological features. With regard to the first, it has been shown that it is possible to derive empirically an observational scaling law which is consistent and which is directly related to the source parameter of seismic moment. This capability to scale properly earthquakes in central United States will have a significant impact on magnitude, recurrence, and magnitude vs felt area relationships, and indicates the need of establishing

similar laws appropriate to other regions.

With regard to the latter two problems, it has been shown that the stress distribution implied by the observed focal mechanism solutions is considerably more complicated than has been proposed by such findings as those of Sbar and Sykes (1973).

References

Aki, K. (1972). Scaling law of earthquake source time-function, Geophys. Journ. Roy astr. Soc. 31, 3-25.

Herrmann, R. B. (1974). Surface wave generation by central United States earthquakes, a dissertation submitted to the Graduate School of Saint Louis University.

Nuttli, O. W. (1973). Seismic wave attenuation and magnitude relations for eastern North America, Jour. of Geophys. Res. 78(5), 876-885.

Nuttli, O. W., and J. E. Zollweg (1974). The relation between felt area and magnitude for central United States earthquakes, Bull. Seism. Soc. Am. 64, 73-86.

Nuttli, O. W. (1974) Magnitude recurrence relation for central Mississippi Valley earthquakes, for publication in the Bull. Seism. Soc. Am. 64 (in press).

Oetking, P. (compiler) (1966). Geological highway map of the mid-continent - no. 1. (American Association of Petroleum Geologists)

Sbar, M. I., and L. R. Sykes (1973). Contemporary compressive stress and seismicity in eastern North America: An example of intra-plate tectonics, Geol. Soc. Amer. Bull. 84, 1861-1882.

3. The Q Structure above the Subduction Zone in South America.

by Rama Somayajulu

Lateral differences in the anelasticity of the earth is a factor which affects strongly the attenuation of seismic waves, and hence the magnitude values determined from seismic amplitudes recorded at seismograph stations. A determination of the lateral variations in the Q structure of the earth is thus an important study for understanding the factors affecting earthquake magnitudes. The present study is an investigation of the anelasticity in a particular type structure, the region above the Nazca Plate in the vicinity of the Peru-Chile border beneath the coast of South America.

There are two classical approaches to find the attenuation from seismic body waves. The first is to measure and correlate the amplitudes of the same phase from station to station. The second is to determine the amplitude ratio of two different phases from the same source recorded at the same station. The former method involves corrections for the source, the instrument, the receiver crust, and the wave paths. In the latter method it is possible to avoid some of these corrections, namely, those for the instrument and receiver crust, and sometimes for portions of the wave path. Many authors have applied this latter method, using the spectral ratios of the direct P or S phase and the phase transmitted and/or reflected at the core boundary

or at the surface of the earth (Kanamori, 1967; Sacks, 1969; Niazi, 1971; Kovach and Anderson, 1964; Steinhart et al., 1964; etc.)

The method followed in this study is to examine the spectral ratio of successive pP and P phases observed at many stations from the same source. For deep focus earthquakes and for epicentral distances greater than 60^{o}, the direct P wave travels wholly in the mantle, whereas the first segments of pP phase traverse the crust and upper mantle above the source twice before travelling a path through the mantle similar to the direct P wave. We assume 1) that the spectral difference between pP and P, after correction for geometric spreading and energy transfer at the surface, is produced by the dissipation properties of the crust and upper mantle above the source, and 2) that the ray P and that portion of pP below the depth of the focus encounter identical Q structure in the mantle and at the receiving station.

Method of Analysis

The method of analysis is described by Niazi (1971). Briefly, let us denote the spectral amplitudes of P and pP by A_1 and A_2, respectively. These amplitudes are functions of the angle of incidence i, and angular frequency w. We assume Q is independent of frequency (Anderson and Archambeau, 1964; Knopoff, 1964). We may write their dependence on the various source and path elements (Fig. 1) as follows.

Now

$$A_1(w,i,\phi) = S_1(i,\phi)\, G_1(i)\, C_1(i,w)\, I_1(i,w) \qquad (1)$$

$$A_2(w,i,\phi) = S_2(i,\phi)\, G_2(i)\, C_2(i,w)\, I_2(i,w)\, R(i,w)\, e^{-KD} \qquad (2)$$

where S_1, S_2 are the effect of radiation

G_1, G_2 are the geometric spreading

C_1, C_2 are the effect of crust and upper mantle excluding the portion of pP (ACD, Fig.1) path above the focus.

R is the reflection coefficient of the shell above the focus

D is the distance ACD along the ray above the focus

K is the average attenuation above the focus

$K = \pi / \alpha T Q$

Q^{-1} specific attenuation coefficient

i is the angle of incidence at the source

ϕ is the bearing of the ray at the source

T is the travel time along the path ACD

α the longitudinal wave velocity.

Since for deep focus earthquakes recorded at larger epicentral distances pP and P traverse virtually the same upper mantle and station crust (by assumption 1), and are recorded by the same instrument, $C_1 \cong C_2$, $I_1 \cong I_2$.

Thus amplitude ratio is expressed

$$\frac{A_2}{A_1} = \frac{S_2\ G_2\ R\ \ Exp(-KD)}{S_1 G_1}$$

$$\log_e \left(\frac{A_2}{A_1}\right) = \log_e \left(\frac{S_2 G_2 R}{S_1 G_1}\right) \quad -KD \qquad (3)$$

The geometrical spreading can be computed for a particular ray path from the following expression (Bullen, 1963)

$$G = \sqrt{\frac{\text{Sin } \theta}{r^2 \text{Sin } \Delta \cos\ \theta_o} \left| \frac{d\theta}{d\Delta} \right|}$$

where r is the radius of the earth

Δ epicentral distance

θ angle that ray leaves the source

θ_o the angle of emergence of ray at the earth's surface .

The geometric spreading for P and pP are small. The reflection coefficient at the surface is computed by using the Thomson-Haskell matrix method (Haskell, 1962). A complete computer program for determining the pP and P travel times, geometric spreading, and energy partition has been written in order to make comparison for energy which has followed pP and P paths. The above program makes use of a multilayered system, where the velocity in each layer is described by a power law of the form $V = ar^b$ (Mohorovicic law) with a and b constants (Herrin et al. 1968). Rewriting

equation 3 and substituting for K and D

$$\log_e \left(\frac{A_2 S_1 G_1}{A_1 S_2 G_2 R} \right) = -KD$$

$$= \frac{-\pi}{\bar{Q}} f \int_D \frac{ds}{\alpha} \qquad (4)$$

where $\bar{Q}$ is the average value of Q for the crust and upper mantle above the focus. We may also write equation (4) as

$$\log_e \left(\frac{A_2 S_1 G_1}{A_1 S_2 G_2 R} \right) = bf \qquad (5)$$

where

$$b = \frac{-\pi}{\bar{Q}} \int_D \frac{ds}{\alpha} .$$

Hence, the spectral amplitude ratio, after correcting for the geometric spreading, reflection at the surface and the effect of radiation, is a function of frequency with a negative slope. The integral, $\int_D ds/\alpha$, in equations (4) or (5) corresponds to the time taken by the P wave to reach the reflecting point at the free surface and to return to the level of the focus. This value can be readily read from the above computer program.

More precisely, the slope of the graph of the logarithm of the corrected spectral ratio versus frequency is equal to (Buchbinder, 1972)

$$b = -\frac{\pi}{Q} \int_{pp'} \frac{ds}{\alpha} - \frac{\pi}{Q} \int_{PP'} \frac{ds}{\alpha} + \frac{\pi}{Q} \int_{P} \frac{ds}{\alpha} \qquad (6)$$

where the integral path pP+ is the path $\overline{ACD}$ (Fig. 1) of pP above focus pP- in the path $\overline{DB}$ of pP below focus, and P is the path $\overline{AB}$ of P. At the large epicentral distances ($> 60^{\circ}$) the radii of penetrations to P and pP differ by approximately 250 kms, where both the rays traverse the lower mantle. By the assumption 2, the last two terms in equation (6) will be approximately equal to one another. Then

$$b = -\frac{\Pi}{Q} \int_{pP+} \frac{ds}{\alpha} = -\frac{\Pi}{Q} T.$$

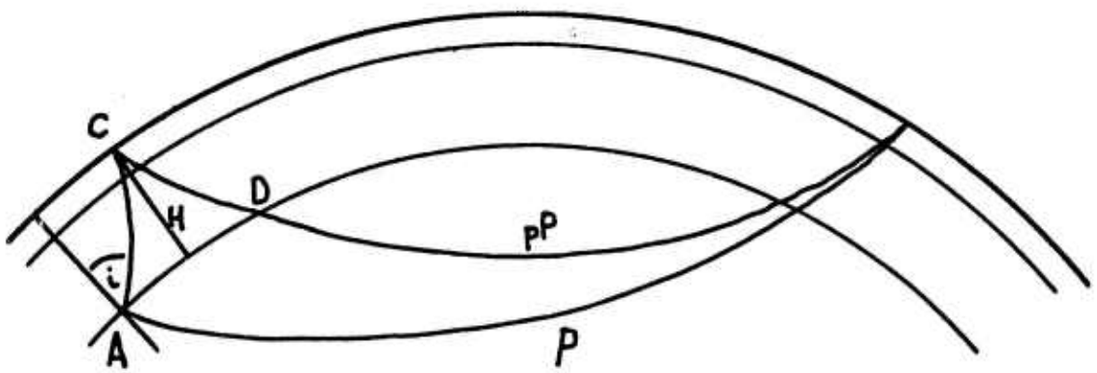

Figure 1. Path of P and pP. $\overline{ACD}$ is the path of integration for pP_+ .

Data

Table 1(see also Fig. 2) lists the earthquakes and recording stations used in this study. The selection of the stations was based on the azimuthal distribution and on the availability and clarity of the records. The hypocenters are located in the zone of deep focus earthquakes in Central Chile. This zone lies beneath the familiar 'Quiet' zone (250-550 kms depth) for earthquakes under Chile. The region above the hypocenters is one in which the dip of the Benioff zone changes, with a possible splitting of the descending plate into two or more tongues (Stauder, 1973).

The data used are taken from long-period vertical seismograms only of WWSSN stations distributed across the United States. The onset of the pP phase is approximately two minutes after the beginning of the P phase at these stations and for the earthquakes selected. Amplitude spectra for the P and pP phases were computed using a Fast Fourier Transform program. Since the time difference between P and pP is small, we can assume that in taking the ratio for the two phases the noise spectra will cancel out.

The spectral amplitudes were corrected for radiation effect, geometric spreading, and reflection at the surface. The corrected spectral ratios (ApP/Ap) were plotted against the frequency on a semi-logarithmic paper. Regression lines were then determined in order to obtain the best fit through

Table 1.

Date	Origin Time	Location	Depth	Magnitude	Station
Aug 23, 68	$22^h36^m51.3^s$	$22^\circ S$ $63.5^\circ W$	537	5.8	BKS, TUC, DUG, ALQ, GOL, LUB, SHA, OXF, BLA, SCP, WES.
Sept 29, 62	15 17 47.6	27.1 63.5	577	6.5	DUG, ALQ, LUB, DAL
Sept 9, 67	10 06 44.1	27.7 63.1	578	5.8	BKS, GSC, TUC, DUG ALQ, FLO, SCP, SBA.
Dec 9, 64	13 35 42.4	27.5 63.2	586	5.9	GSC, GOL, AAM, BCA, ATL
Jan 17, 67	01 07 54.3	27.4 63.3	590	5.5	ALQ, GOL, BLA.

Figure 2. Source locations, and path relationships to recording sites.

the points. The slope, b, of the line is equal to the integral term, $-\frac{\pi}{Q}\int_D dS/\alpha$, in equation (5). Thus, given the value of b, $\bar{Q}$ can be calculated for each earthquake at each station.

The calculated mean Q values so obtained are listed in Table 2. Fig. 3 illustrates these same values together with error bars indicating the standard deviations.

Event I has $\bar{Q}$ values which vary from 100 to 580. Events II and III yield $\bar{Q}$ values with slightly larger variations, from 16 to 600. For event IV the values are fairly uniform, ranging only from 200 to 360. Finally, for event V $\bar{Q}$ takes on values notably higher than in the other cases, ranging from 560 to 1440.

In Table 2 and in Figure 3 the receiving stations are ranged from west to east, numbers 1-6 corresponding to those in the western United States, numbers 7-17 to those in the eastern United States. Examination either of the table or the figure shows that the $\bar{Q}$ values determined from stations in the western United States are both lower, on the average, and more erratic than those determined from stations in the eastern United States. While the reflection point of pP and the precise ray path of pP relative to the position of the slab are not here presented, reference to Fig. 1 indicates that the p segment of pP paths for the western stations passes through a zone just above the upper surface of the descending oceanic plate, whereas for stations to the east this segment of the pP path travels through greater

Table 2

No.	Stn.	I Aug 23, 68 (537 km)			II Sept 29, 62 (577 km)			III Sept 9, 67 (578 km)			IV Dec 9, 64 (586 km)			V Jan 17, 67 (590 km)		
		Q_M	Q_U	Q_L	Q_M	Q_U	Q_L	Q_M	Q_U	Q_L	Q_M	Q_U	Q_L	Q_M	Q_U	Q_L
1	BKS	296.0	455.6	219.2				141.0	171.6	119.6						
2	GSC							72.0	75.8	68.6	259.0	449.4	181.8			
3	TUC	128.4	137.0	120.6				41.6	43.0	40.2						
4	DUG	216.8	266.8	182.6				131.0	298.6	184.2						
5	ALQ	250.2	341.2	197.4	149.6	167.2	135.0	87.2	96.4	79.8				556.2	762.8	437.6
6	GOL	404.8	640.6	295.8							358.8	457.6	295.0	1436.8	2311.6	1042.2
7	LUB	96.8	101.2	92.8	210.2	241.2	186.2									
8	DAL				611.8	851.0	477.4									
9	SHA	273.2	383.4	212.2												
10	FLO							343.0	426.6	289.6						
11	AAM										314.8	404.6	257.6			
12	OXF	285.0	425.6	214.2												
13	BLA	572.0	1010.0	399.0							241.6	335.6	188.6			
14	ATL										201.2	222.6	183.7			
15	SCP	262.6	363.6	205.6												
16	WES	555.0	707.8	456.2												
17	SBA							411.2	631.0	304.8						

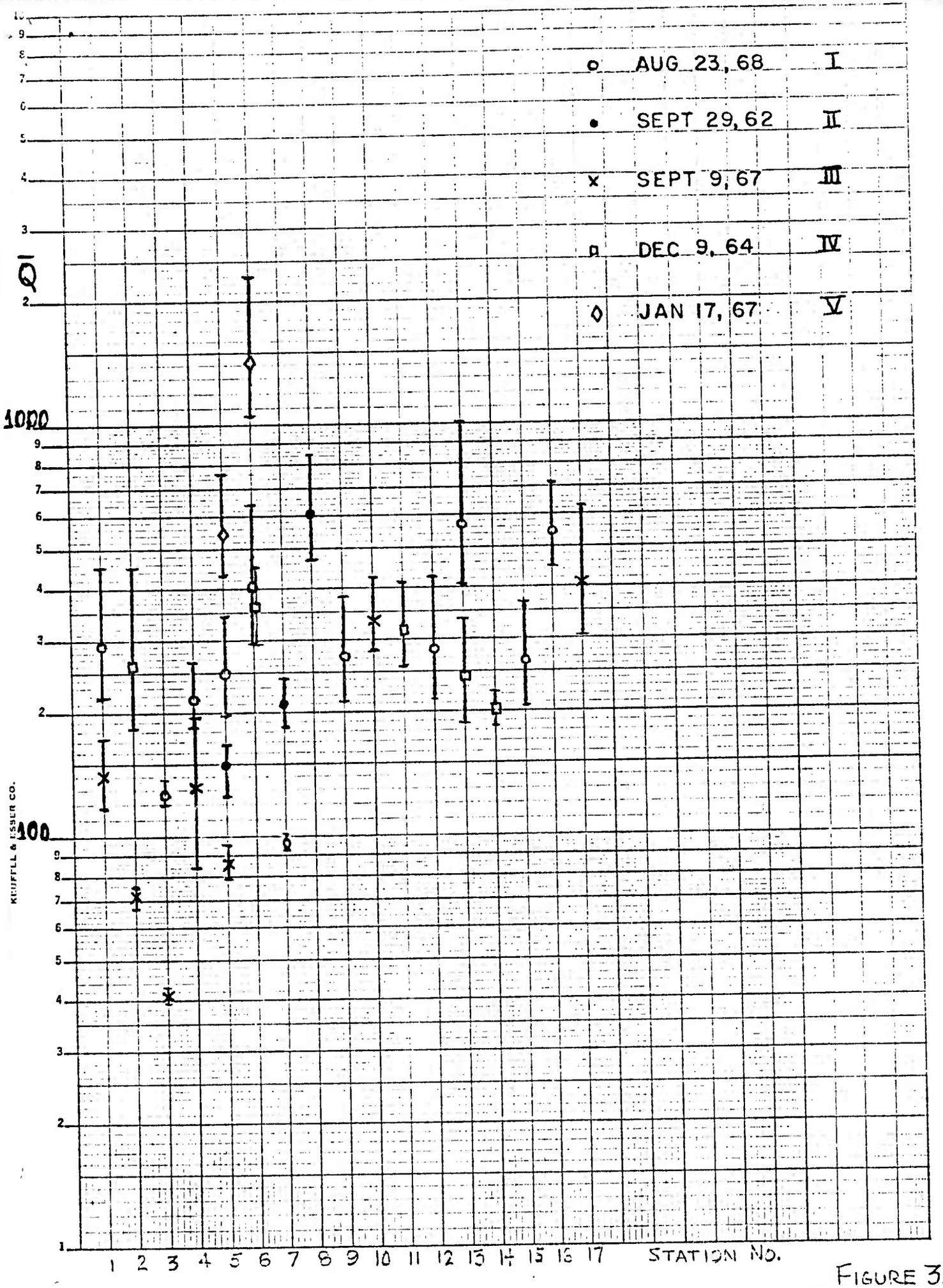
AUG 23, 68 I
SEPT 29, 62 II
SEPT 9, 67 III
DEC 9, 64 IV
JAN 17, 67 V
Q̄
1000
100
STATION NO.
1 2 3 4 5 6 7 8 9 10 11 12 13 14 15 16 17
KEUFFEL & ESSER CO.

FIGURE 3.

portions of the wedge (aseismic in this portion of South America) between the descending plate (or segment of palec plate) and the continental plate. Evidence from seismicity and focal mechanisms (Stauder, 1973) shows that the former path is likely to be one of greater heterogeneity, for the plate is probably segmented and irregular in its relief, thus accounting for the lower $\overline{Q}$ values and the scatter in the $\overline{Q}$ values.

The values of $\overline{Q}$ from stations in eastern United States, while more uniform, are relatively low ($\overline{Q}$ = 300 to 400). This indicates passage through a low velocity layer of considerable vertical extent from the source region of 600 km depth to the lithosphere. Sacks and Okada (1973) found Qp values in excess of 1000 generally to prevail in the wedge, above the descending Nazca plate at depths down to 350 km, but low values of Qp below this level. The values reported here are average values for the entire region above the source level at 600 km depth, and were obtained from a double passage (pP + path above) through the portion of mantle in question.

References

Buchbinder, C.R.G. (1972). Comments on paper by Mansour Niazi "Seismic dissipation in deep seismic zones from spectral ratio of pP/P", J. Geophy. Res. 77, 1586-87.

Bullen, K. E. (1963). Introduction to Seismology, Cambridge Univ. Press.

Haskell, N. E. (1962). Crustal reflection of P and SV waves, J. Geophy. Res. 67, 4751-

James, D. E. (1971). Andean crustal and upper mantle structure, J. Geophys. Res. 76, 3246-3271.

James, D. E., and I. S. Sacks (1969). Upper mantle structure beneath western South America. Carnegie Inst. Yearbook 67, 353-357.

Kanamori, H. (1967). Attenuation of P waves in the upper and lower mantle, Bull. Eq. Res. Inst., Univ. of Tokyo, 45, 299.

Kovach, R. L., and D. L. Anderson (1964). Attenuation of shear waves in the upper and lower mantle, Bull. Seism. Soc. Am. 54, 1855-1864.

Niazi, M. (1971). Seismic dissipation in deep seismic zones from spectral ratio of pP/P, J. Geophys. Res. 76, 3337-3344.

Sacks, I. S. (1963). A lossy low-velocity layer in the mantle, Carnegie Inst. Yearbook 62, 286-288.

Sacks, I. S. (1967). Distribution of absorption of shear waves in S. America its tectonic significance, Carnegie Inst. Yearbook 67, 339.

Sacks, I. S., and H. Okada (1973). A comparison of the anelastic structure between western South America and Japan, Carnegie Inst. Yearbook 72, 226-233.

Stauder, W. S. (1973). Mechanism and spatial distribution of Chilean earthquakes with relation to subduction of the oceanic plate, J. Geophys. Res. 78, 5033-5061.

Steinhart, J. S., T. J. Smith, I. S. Sacks, R. Sumner, Z. Suzuki, A. Rodriguez, C. Lomnitz, M. A. Tuve, and L. T. Aldrich (1964). Seismic studies, Carnegie Inst. Yearbook 62, 280-289.